High-power Terahertz Waves for a Recycle System of Amyloid Fibrils

Takayasu Kawasaki (takayasu.kawasaki@kek.jp)
Accelerator Laboratory, High Energy Accelerator Research Organization
Yuusuke Yamaguchi
Research Center for Development of Far-Infrared Region, University of Fukui
Hideaki Kitahara
Research Center for Development of Far-Infrared Region, University of Fukui
Akinori Irizawa
The Institute of Scientific and Industrial Research, Osaka University
Masahiko Tani
Research Center for Development of Far-Infrared Region, University of Fukui

Research Article

Keywords: persistent materials, scanning-electron microscopy, small-angle X-ray scattering, fibrous biomaterials

Posted Date: August 5th, 2021

DOI: https://doi.org/10.21203/rs.3.rs-767284/v1

High-power terahertz waves for a recycle system of amyloid fibrils

Takayasu Kawasaki[1,2]*, Yuusuke Yamaguchi[3], Hideaki Kitahara[3], Akinori Irizawa[4], and Masahiko Tani[3]

[1] IR Free Electron Laser Research Center, Tokyo University of Science, 2641 Yamazaki, Noda, Chiba 278-8510, Japan.

[2]Accelerator Laboratory, High Energy Accelerator Research Organization, 1-1 Oho, Tsukuba, Ibaraki 305-0801, Japan.

[3]Research Center for Development of Far-Infrared Region, University of Fukui, 3-9-1 Bunkyo, Fukui, Fukui 910-8507, Japan.

[4] The Institute of Scientific and Industrial Research, Osaka University, Mihogaoka 8-1, Ibaraki, Osaka 567-0047, Japan.

*Correspondence to: takayasu.kawasaki@kek.jp

Abstract

Recycling of persistent materials is one of most important subjects to be addressed towards the sustainable society. Amyloid fibril is such a tough biomaterial that can be designed for various industrial applications, and it is usually difficult to dissociate the once made fibrous conformation due to the cross β-sheet stacks. We propose here a unique but versatile approach to handle the fibril formation by using two-kinds of high-power terahertz waves. Lysozyme and β2-microglobulin peptide fragment were employed as model samples, and those fibrils were clearly disaggregated accompanied by decrease of β-sheets and increase of α-helices by the irradiation of 5.3 THz free electron laser tuned to 56 μm, as shown by infrared (IR) microscopy and scanning-electron microscopy (SEM). In contrast, those fibrous conformations were reversely self-associated by the irradiation of 0.42 THz wave tuned to 720 μm from gyrotron, as shown by optical and IR microscopies, SEM, and small-angle X-ray scattering. The overall reaction is performed at room temperature within 30 min without external heating and high-pressures. Therefore, amyloid fibrils can be dissociated and associated under the proper far-infrared radiation conditions, which inspires a sustainable recycling system of fibrous biomaterials.

In recent years, fiber-type biomaterials have attractive attentions in various industrial fields[1-14]. As a representative biomaterial, cellulose nanofiber can be developed for cosmetic additives[1], anti-bacterial sheets, and porous materials in healthcare and pharmaceuticals fields[2,3], and for components of electronic devises and auto parts in mechanical industries[4,5]. As with the cellulose, amyloid fibrils can also be utilized as functional biomaterials. The amyloid is originally well-known to be involved in various biological phenomena such as the onset of serious amyloidosis[6,7], biofilm formation[8,9], biosynthesis of pigment melanin[10], protection of eggshells[11], supramolecular assembly in the body structures[12], and gene expressions[13]. On the contrary, the amyloid-like proteins and peptides can be on-demand designed based on the solid-phase peptide synthesis technique[14-16], which allows us to develop various amyloid materials such as rigid scaffolds for cell cultivation and tissue engineering[17,18], artificial capsules and hydrogels for drug delivery systems[19,20], and functional nanofilms for microorganism adhesion and protein crystallization for medical purposes[21,22]. Therefore, a versatile approach for structural control of the amyloid fibrils will be useful for remodeling of the fibrous format in various biomaterial fields. However, the cross β-sheet stacking structure, that is common in amyloid fibrils, is hydrophobic and stable in water, which makes it difficult to regulate the once made fibril freely[23,24]. Of course, organic solvents such as dimethyl sulfoxide are known as the melting reagent, and fibril binding molecules are explored for modulating the fibril formation[25-27]. Nonetheless, for the most part, it may be

55 difficult to regenerate the amyloid materials from the complex mixture with the other ingredients.
56 Regarding the physical stimulation methods, external electric and magnetic fields[28],
57 microwaves[29,30], and ultrasonication[31,32] have been investigated for the specific modification of
58 proteins. Nonetheless, these approaches have merits and demerits in terms of versatility,
59 conveniences, and economical aspects, and more efficient approaches will be desired for the
60 construction of sustainable recycle system of the persistent biomaterials.
61 Here, we show a unique but widely applicable way using intense terahertz waves to dissociate
62 and re-associate the amyloid fibrils under mild conditions. In **Fig. 1a**, frequencies and
63 wavelengths of lights (upper) and various parameters of the oscillation systems used in this study
64 (below) are shown. The terahertz region is usually ranged from 30 to 3000 μm wavelengths and
65 is applied for various studies such as terahertz spectroscopy[33], terahertz radiation[34], and spectral
66 imaging[35]. We employed two kinds of rays, terahertz free electron laser (THz-FEL)[36] and a
67 submillimeter wave from gyrotron[37]. The THz-FEL has double pulse structure that is composed
68 of micropulse and macropulse in which the duration of the former is 10-20 ps and that of the latter
69 is 4 μs. The oscillation wavelength is covered from 30 to 300 μm, and the irradiation power is
70 given as avg. 5 mJ per macropulse. The THz beam can be oscillated briefly as follows (**Fig. 1b)**:
71 an electron beam is accelerated to near photon rate by a linear accelerator, and the accelerated
72 electron beam goes into the periodic magnetic field, under which an FEL pulse can be amplified

in the optical cavity consisting of two spherical mirrors. A fraction of the FEL pulse is taken out through a coupling hole in the upstream mirror and led to the monochromator to produce a coherent light. The submillimeter wave from gyrotron is a single pulse (1- 2ms half width) having 10 W power and is generated as follows (**Fig. 1c**): a helical electron beam is extracted from a thermal cathode electron gun and repeats cyclotron motion in superconducting magnet. The motion energy is converted into the electromagnetic energy in the cavity resonator, and the electromagnetic wave is radiated as Gaussian beam into the laboratory through the internal mode converter and mirrors. The gyrotron oscillation system nowadays acts as a strong radiation source for the nuclear magnetic resonance (NMR) spectroscopy with the dynamic nuclear polarization (DNP) technique[38-40]. In addition, the hyperthermia treatment using the terahertz radiation is expected to be a candidate for the therapeutic strategy for cancer[41,42].

In this study, we employed lysozyme from hen egg white and β2-microglobulin peptide fragment from human as model samples, and those fibrils were irradiated by the THz-FEL and submillimeter wave from gyrotron under atmosphere. The all radiations proceed at room temperature without any external heating and high-pressures.

Dissociation of amyloid fibers

At first, the irradiation effect by THz-FEL is described. **Figure 2a** shows far-infrared spectra of

91 lysozyme and β2-microglobulin from 130 to 250 wavenumbers (cm^{-1}), and both samples exhibit
92 strong absorption peak at about 170-190 cm^{-1} (52.6-58.8 μm) and weak absorption peaks at 130-
93 150 cm^{-1} (66.7-76.9 μm). After each sample was fibrillated by thermal incubation and spotted on
94 the slide base, the FEL beam was tuned to 56 or 70 μm and introduced onto the dried sample for
95 10 min (=3000 macropulses). In **Fig. 2b**, the result by infrared absorption spectral analysis was
96 shown. In case of lysozyme fibril, there are two bands at amide I region before irradiation (black
97 line, left panel), and the irradiation at 56 μm (red line) gave decrease of the peak intensity at lower
98 wavenumber (ca. 1620 cm^{-1}) and increase of that at higher wavenumber (ca. 1650 cm^{-1}). Since
99 the amide I band at the lower wavenumber corresponds to β-sheet structure and the latter band
100 influences α-helix or non-fibrous conformation[43], the spectral change by the irradiation at 56 μm
101 indicates the decrease of the β-sheet rich conformation. The protein structure analysis based on
102 the analytical software[44] (right panel) proved that the proportion of β-sheet decreased from 45%
103 before irradiation (black bar) to 20% after irradiation (red bar) and that of α-helix increased from
104 5% (black bar) to 30% (red bar). On the contrary, the irradiation at 70 μm (green line and bar)
105 also decreased β-sheet and increased α-helix, but the degrees of those changes are not remarkable.
106 In case of β2-microgobulin, a strong band and a shoulder peak were observed at 1617 cm^{-1} and
107 at 1655 cm^{-1} before irradiation (gray line), respectively. The irradiation at 56 μm gave the increase
108 of the latter peak intensity (blue line), increase of proportion of α-helix from 5% (gray bar) to

40% (blue bar), and decrease of β-sheet from 50% to 5%. The irradiation at 70 μm gave the similar tendency (brown), but the effect is not remarkable compared to 56 μm.

Figure 2c showed the SEM observation before (-) and after (+) the THz-FEL irradiation. Assemblies consisting of many strings (several nanometers in width and several micrometers in length) in lysozyme fibril (upper, left) were destroyed accompanied by crushing of sodium salts (upper, right). Soft-cloth like fibrils of β2-microglobulin (about two hundred nanometer in width and several micrometers in length) were also dissociated by the irradiation (below).

These analytical results indicated that the THz-FEL irradiation can dissociate the amyloid fibril structure by decreasing β-sheets and increasing α-helices.

Promotion of amyloid self-association

Next, we describe about the effect of a submillimeter wave from gyrotron. **Figure 3a** shows temperature on the surface of the sample tube during the irradiation. Prior to the irradiation experiments, we confirmed that the transmittance of the terahertz wave against the sample tube was more than 80% at 0-2.0 THz region (**Fig. S1**). In case of 10 W power with 1 ms pulse duration, temperature reaches about 27. 5 ℃ on both at cover and bottom of the tube for 20 min, and the temperature at the bottom was slightly increased and that on the cover decreased in case of 2 ms pulse duration. Therefore, at the present irradiation conditions, the temperature increase is only

around 5 K compared to the non-irradiation area. The low-resolution microscopy observation (**Fig. 3b**) showed that the fibrous aggregate was observed like black-brown colors in both lysozyme and β2-microglobulin before the irradiation (0 mJ). When the irradiation power was increased from 10 mJ (10 W with 1ms pulse duration) to 20 mJ (10 W with 2 ms pulse duration), the black-brown colors were apparently concentrated in both cases (white totted circles). The high-resolution electron microscopy observation showed that the fibril structure changed into more solid aggregates by the irradiation at 20 mJ power in both samples (**Fig. 3c**). In case of lysozyme, needle-like fibrils (several hundred nanometer in width, several micrometers in length) were sparse without irradiation (-), and thick branch-like fibrils (one micrometer in width, several micrometers in length) were increased with the irradiation (+). In case of β2-microglobulin, the assemblies of many strings (several hundred nanometer in width, ten to twelve micrometers in length) before the irradiation (-) were clearly changed into bundles like clay after the irradiation (+).

Figure 3d shows results by infrared absorption spectral analysis. In case of lysozyme (upper, left panel), the peak intensity at around 1620 cm^{-1} was apparently increased after the irradiation (red) compared to that before irradiation (black). The protein structure analysis (right panel) indicated that β-sheet was increased, and α-helix was decreased by the irradiation[44]. In case of β2-microglobulin (below, left panel), the peak intensity at 1623 cm^{-1} before irradiation (gray) was

145 obviously increased accompanied by increase of proportion of β-sheet (right panel) after the
146 irradiation (blue).

147 The result by SAXS analysis was shown in **Fig. 3e**. In both cases, the inclination of the scattering
148 curve from 3 nm^{-1} to 9 nm^{-1} was larger after the irradiation (red) than that before irradiation (black).
149 This means that the shape of the aggregate was changed into the thick lamellar type[45]. In addition,
150 there can be observed a scattering peak at around 3.8 nm^{-1} in lysozyme (upper) and at 3.7 nm^{-1} in
151 β2-microglobulin (lower) after irradiation. These peaks mean that a size (d) of layer of the fibril
152 is 1.65 nm and 1.69 nm, respectively. These values are quite larger than the typical size (0.9-1.0
153 nm) of the amyloid fibril [46].

154

155 **Recycle of fibrous biomaterials by the far-infrared radiation**

156 The above all results suggested that the fibrous conformations of lysozyme and β2-
157 microglobulin were dissociated by the THz-FEL and associated by the submillimeter wave from
158 gyrotron. This study implied that dissociation and association of amyloid fibrils can be performed
159 in one batch system by using terahertz waves properly at different wavelengths (**Fig. 4**). By using
160 both terahertz radiations continuously, the amyloid-base fiber biomaterials can be recycled
161 without denature of the protein backbone. This method requires no organic solvents, no external
162 heating, and no high pressures, which inspires that the electromagnetic waves at terahertz region

will become a green technology for the sustainable system of fibrous biomaterials. We demonstrated that the submillimeter wave can promote the fibril formation of many kinds of amyloid peptides (GNNQQNY, $A\beta_{1-40}$, SAA, and DFNKF in our previous study[47], lysozyme and β2-microglobulin in the present paper), and in every case, β-sheet conformation was dominated and the sample was more aggregated than the pre-irradiation state. Nonetheless, the reformed aggregate seems to be shapely larger and more rigid than the pre-irradiation state (**Fig. 3c, e**). Therefore, it can be implied that the submillimeter wave from gyrotron will be a versatile tool for remodeling of amyloid-base fiber biomaterials, and this method will be potentially applied for modifying other fibrous materials such as cellulose nano-fibers[1-5] to improve the fibrous characteristics such as the rigidness and the regularity.

Previously, we reported that the THz-FEL can dissociate an amyloid fibril from calcitonin DFNKF peptide[48]. Together with this prior study, it was revealed that several kinds of amyloid fibrils can be dissociated by the THz-FEL. The tendency of decrease of β-sheets by the irradiation was varied dependent on the molecular size of amyloid: the proportion of the β-sheet of DFNKF was decreased from 40% to 10%[48], that of β2-microglobulin was from 50% to 5%, and that of lysozyme was from 45% to 20% (**Fig. 2b**). Therefore, smaller sized peptides (5 a.a. of DFNKF and 11 a.a. of β2-microglobulin) may be easier to be dissociated than the larger sized protein (129 a.a. of lysozyme). Although the detailed mechanism is not clear at the present stage, it can be

181 considered that the dissociation process may be similar with the phenomenon under which a solid
182 aggregate is momentarily unraveled in boiling water. As one of experiments to investigate the
183 reaction mechanism, it can be planned to monitor the dissociation processes by using atomic force
184 microscopy in the presence of fibril-binding molecules[49]. This experiment will be a next
185 challenging theme. As a side application, THz-FEL can be applied to the amyloidosis therapy by
186 reducing pathogenic amyloid aggregates from tissues in surgical medicine, and to regulate the
187 growth of microorganisms by suppressing the biofilm formation related with amyloids in
188 synthetic biology. These themes are also fascinated as application studies of the terahertz rays.
189
190 **Conclusion**
191 We proposed here that fibrous biomaterials can be recycled by using two-kinds of high-power far-
192 infrared rays. One is THz-FEL that is accelerator-based picosecond pulse laser, and another is a
193 submillimeter wave from gyrotron. Lysozyme and β2-microglobulin peptide fragment were
194 employed as models, and THz-FEL tuned to 56 μm can dissociate those stacking conformations
195 accompanied by decrease of β-sheet and increase of α-helix, and the submillimeter wave at 720
196 μm can promote those fibrillations reversely, as revealed by infrared, electron, and optical
197 microscopies, and SAXS analyses. The total elapsed time is within 30 min, and those radiations
198 can be performed at room temperatures without any external heating and high-pressures.

Combination of these far-infrared radiations will be expected to contribute to a sustainable recycle system of the fibrillar biomaterials in future.

Methods

Materials

Lysozyme (from hen egg white) was purchased from Sigma-Aldrich (Tokyo, Japan). β2-Microglobulin (21-31, NFLNCYVSGFH) was purchased from PH-Japan (Hiroshima, Japan). Acetic acid and sodium chloride were purchased from Wako Pure Chemical Industries (Osaka, Japan).

Sample preparation

As for THz-FEL irradiation, lysozyme and β2-microglobulin were fibrillated as follows: Lysozyme powder was dissolved in 20 % acetic acid (2.5 mg/mL) containing sodium chloride (0.5 M), and the solution (1 mL) was incubated for 20 h at 37 ℃. The freeze-dried β2-microglobulin peptide was dissolved in dimethyl sulfoxide (40 mg/mL) and stocked at -20 ℃. The portion of the stock solution was diluted by phosphate buffer saline (pH 7.5) containing sodium chloride (100 mM) to be 2.0 mg/mL concentration and incubated at 37 ℃ for two days. Those suspensions (each 10 μL) were spotted on a stain less steel base for infrared microscopy or a glass slide base for scanning-electron microscopy observation. After drying under atmosphere,

those samples were irradiated by THz-FEL.

As for gyrotron experiments, samples were prepared as follows: Lysozyme was dissolved in acidic water (150 μL) as described above, and the solution was used for the irradiation experiment without the subsequent thermal incubation. A portion of the stock solution of β2-microglobulin peptide was diluted by the buffer as described above, and the solution was directly subjected to the irradiation experiment without further incubation.

THz-FEL irradiation

The principle of the beam generation was briefly as follows: an FEL oscillation system consists of an electron gun, sub-harmonic buncher, an accelerator tube, a periodic magnetic field (wiggler in this case), and an optical cavity to amplify the FEL pulses. A small portion of the FEL pulses in the cavity is extracted via a coupling hole that is 3 mm in diameter at the center of the upstream resonant mirror. The wiggler is the Halbach-type magnetic field. The FEL beam is transported through a concrete wall (3 m in thick) and through a diamond window of the monochromator to the experimental room. The oscillation wavelengths were tuned to 56 or 70 μm, and the amyloid sample dried on a slide base was irradiated by the THz-FEL from the vertical direction at room temperature with raster scan. Under this irradiation conditions, beam diameter was focused to approximately 400 μm by using a parabolic reflector, the irradiation area was 1 mm x 1mm square, and the step scan length was set to 0.1 mm.

Gyrotron irradiation system

The gyrotron is a vacuum electron tube and the operation is based on a physical phenomenon known as electron cyclotron maser instability. The structure is composed of an electron-optical system based on a triode magnetron injection gun with a thermionic cathode that generates a helical electron beam in the superconducting magnet, a cavity resonator for coupling the electron beams with waves, an internal mode converter to adjust spatial distributions of oscillated waves, an output vacuum window, and a water-cooled collector of the spent electron beams. The submillimeter wave can be oscillated as Gaussian wave beam from the output vacuum window. We used the Gyrotron FU CW GVIB far-infrared radiation system, which can expose samples to a 420 GHz wave with 10 W power for 20 min. The radiation wavelength was 720 μm, and the pulse duration was 1 ms or 2 ms at 5 Hz repetition. The temperature increase of the sample during the irradiation was monitored using a Testo 875 thermography camera (Testo). The amyloid sample in aqueous solution (150 μL) was put on the Eppendorf tube that is composed of polypropylene and was irradiated at room temperature (ca. 25 °C) from vertical direction.

Terahertz spectroscopy

We used a far-infrared Fourier-transform spectrometer (IFS66v/S, Bruker) for the absorption spectrum measurement at terahertz region. The sample powder was mixed with CsI powder and pressed to form a mini-disk plate. The measurement was performed by transmission mode, and

253 the spectrum was recorded at 130-700 cm^{-1} with 32 scans using Mylar (polyester film) as beam
254 splitter.

255 **Infrared microscopy**

256 The mid-IR spectra were measured using IRT-7000 infrared microscope (Jasco Co, Tokyo, Japan)
257 and FT/IR-6100 spectrometer (Jasco Co., Tokyo, Japan). The dry surface of the sample film was
258 observed by 16x Cassegrain lens, and the infrared spectra were recorded by a reflection mode
259 with 64 scans and 4 cm^{-1} resolution. For analysis of protein secondary structure, we used IR-SSE
260 analytical software (Jasco Co., Tokyo, Japan) in which calibration curve data was prepared as a
261 standard data file by multicomponent analysis (Partial Least Squares quantification model) based
262 on the secondary-structural data of 17 proteins[44]. In this program, the amide I band can be
263 deconvoluted into major four bands: α-helix (1650-55 cm^{-1}), β-sheet (1625-40 cm^{-1}), β-turn
264 (1655-75 cm^{-1}), and other conformation (1645-50 cm^{-1}). Proportions of secondary structures were
265 obtained based on peak intensities at those amide-I bands.

266 **Scanning-electron microscopy**

267 We used FE-SEM Supra40 scanning electron microscope (Carl Zeiss). After the amyloid sample
268 was added on a glass slide base and dried under atmosphere, the slide base was fixed on a sample
269 holder by using conductive copper tape. The surface of the sample was observed using the
270 acceleration voltage at 5.0 kV.

Optical microscopy

The amyloid sample was added on a gold-coated slide base and dried under atmosphere. The surface of the sample was observed using an Area PIII-FX microscope (SK-Electronics Co., LTD., Kyoto, Japan) with a high-magnification object lens (×200–2000). Images were obtained using a 12 million-pixel CCD camera under the halogen lamp. Images of the sample surface were obtained using Perfect Viewer 7 imaging software (SK-Electronics Co., LTD., Kyoto, Japan).

Small-angle X-ray scattering

X-ray scattering experiment was performed using the beamline BL8S3 in Aichi Synchrotron Radiation Center (Aichi, Japan). As for lysozyme, the suspension containing the fibril was put on a Teflon sheet (1mm in depth), and the sample was surrounded and encapsulated by using Kapton tape that is made of polyimide film (TERAOKA SEISAKUSHO CO., LTD., Tokyo). The sample cell was set at the vertical position against the X-ray direction. As for β2-macroglobulin, the suspension was spotted on a cover glass and dried under atmosphere. The cover glass was set at the vertical position against the X-ray direction. In both cases, the wavelength of X-ray was 0.15 nm and the sample-to-specimen length was 45 cm for measurements. The scattering patterns were recorded by use of R-AXIS imaging plate (Rigaku, Japan). Each exposure time of X-ray was 600 s.

Acknowledgements

This work was supported in part by the research program “Dynamic Alliance for Open Innovation Bridging Human, Environment and Materials” (subject number: 20201272), the collaborative research with Research Laboratory for Quantum Beam Science, Institute of Scientific and Industrial Research, Osaka University (subject number: J-11), the collaborative research project of the Research Center for Development of the Far-Infrared Region, University of Fukui, in the fiscal year 2020 (subject number : R02FIRDM028A), and Japan Society for the Promotion of Science KAKENHI (JP20K12483). A part of this work was performed with the aid of Instrument Center, Inst. Mol. Sci. Okazaki (IMS program No. S-20-MS-1077), and we thank Dr. Mikio Uruichi for the operation of far-infrared spectral measurement. The X-ray scattering experiment was performed at Aichi Synchrotron Radiation Center, Aichi Science & Technology Foundation, Aichi, Japan (proposal no. 202005028), and we thank Dr. Kazutaka Kamitani and Dr. Hiroko Yamamoto for the operation.

Author contributions: T.K. designed the study, conducted all analytical experiments, and drafted the manuscript; Y.Y. and M.T performed gyrotron oscillation; H.K performed terahertz spectroscopy; A.I performed the oscillation of FIR-FEL. All authors gave final approval for publication.

Competing interests: The authors declare no competing interests.

Data availability: A part of data is represented as Supplementary Information, and other experimental data are available from the corresponding author (T. K.).

Figure Legends

Fig. 1 Far-infrared rays oscillation systems used in this study. (a) Frequency region of electromagnetic waves (upper) and oscillation parameters of THz-FEL and gyrotron (bottom). (b) Oscillation system of THz-FEL. The system is composed of four parts: linear accelerator (Electron Gun + Sub-Harmonic Buncher + Accelerator Tube), Periodic Magnetic Field, Resonant Mirrors, and outlet of light (Reflective Mirror and Vacuum Beam Port). c) Structural components of gyrotron. The overall structure is briefly composed of five parts: Electron Gun, Beam Tunnel, Cavity Resonator, Internal Mode Converter, and Collector. The submillimeter wave is radiated from Vacuum Window.

Fig. 2 Effect of THz-FEL on amyloid fibrils. (a) THz absorption spectra. Black line: lysozyme fibril; dotted line: β2-microglobulin fibril. (b) Mid-infrared absorption spectral analysis. Left panels: infrared spectra at amide I and II region. Upper: lysozyme, below: β2-microglobulin. Right panel: protein secondary structure analysis. Black: Lysozyme without irradiation; red: Lysozyme with irradiation at 56 μm; green: Lysozyme with irradiation at 70 μm; gray: β2-microglobulin without irradiation; blue: β2-microglobulin with irradiation at 56 μm; brown: β2-

microglobulin with irradiation at 70 μm. (c) SEM observation before (-) and after (+) irradiation. Upper: lysozyme, below: β2-microglobulin. bar: 200 nm.

Fig. 3 Effect of 420 GHz gyrotron on amyloid fibrils. (a) Thermography camera observation. Left: 10 W power irradiation with 1 ms pulse duration, right: 10 W irradiation with 2 ms pulse duration. (b) Optical microscopy observation before (0 mJ) and after irradiations at 10 mJ and 20 mJ powers. Upper: lysozyme, below: β2-microglobulin. Bar: 1 mm. (c) SEM observation before and after irradiation at 20 mJ power. Upper: lysozyme, below: β2-microglobulin. Bar. 1 μm. (d) Mid-infrared absorption spectral analysis after irradiation at 20 mJ power. Left panel: infrared spectra at amide I and II region. Upper: lysozyme, below: β2-microglobulin. Right panel: protein secondary structure analysis. Black: Lysozyme without irradiation; red: Lysozyme with irradiation; gray: β2-microglobulin without irradiation; blue: β2-microglobulin with irradiation. (e) SAXS spectra before and after irradiation at 20 mJ power. Upper: lysozyme, below: β2-microglobulin. d value equals $2\pi/q$.

Fig. 4 A recycle system of amyloid fibrils by using terahertz waves. The fibrous conformation of amyloid fibrils as a representative biomaterial can be dissociated by THz-FEL irradiation and associated by a submillimeter wave from gyrotron.

References

1. Bianchet, R.T., Cubas, A.L.V., Machado, M.M., Moecke, E.H.S., Applicability of bacterial cellulose in cosmetics – bibliometric review, *Biotechnol. Rep*. **27** (2020) e00502. https://doi.org/10.1016/j.btre.2020.e00502

2. Chien, H-W., Tsai, M-Y., Kuo, C-J., and Lin, C-L., Well-Dispersed Silver Nanoparticles on Cellulose Filter Paper for Bacterial Removal, *Nanomaterials* 2021, 11, 595. http://doi.org/10.3390/nano11030595.

3. Qin, C., Yao, M., Liu, Y., Yang, Y., Zong, Y., and Zhao, H., MFC/NFC-Based Foam/Aerogel for Production of Porous Materials: Preparation, Properties and Applications, *Materials* 2020, **13**, 5568; doi:10.3390/ma13235568

4. Wang, X., Yao, C., Wang, F., and Li, Z., Cellulose-Based Nanomaterials for Energy Applications, *Small*. 2017, **13**(42). doi:10.1002/smll.201702240.

5. Zwawi, M., A Review on Natural Fiber Bio-Composites, Surface Modifications and Applications, Molecules 2021, 26, 404. https://doi.org/10.3390/molecules26020404

6. Fändrich, M., Nyström, S., Nilsson, K.P.R., Böckmann, A., LeVine III, H., and Hammarström, P., Amyloid fibril polymorphism - a challenge for molecular imaging and therapy, *J. Intern. Med*. 2018, **283**(3): 218–237. doi:10.1111/joim.12732

7. Chuang, E., Hori, A.M., Hesketh, C.D., and Shorter, J., Amyloid assembly and disassembly, *J. Cell Sci*. (2018) 131, jcs189928. doi:10.1242/jcs.189928

8. Erskine, E., MacPhee, C.E., and Stanley-Wall, N.R., Functional Amyloid and Other Protein Fibers in the Biofilm Matrix, *J. Mol, Biol*. (2018) **430**, 3642–3656. https://doi.org/10.1016/j.jmb.2018.07.026

9. Fowler, D.M., Koulov, A.V., Balch, W.E., and Kelly, J.W., Functional amyloid – from bacteria to humans, Trends Biochem. Sci. 2007, **32**, 5. doi:10.1016/j.tibs.2007.03.003

10. Fowler, D.M., Koulov, A.V., Alory-Jost, C., Marks, M.S., Balch, W.E., Kelly, J.W., Functional Amyloid Formation within Mammalian Tissue, *PLoS Biol*., 2006, **4**(1): e6. DOI: 10.1371/journal.pbio.0040006

11. Siniukova, V.A., Sopova, J.V., Galkina, S.A., and Galkin, A.P., Search for functional amyloid structures in chicken and fruit fly female reproductive cells, *Prion*, 2020, **14**(1), 278–282. https://doi.org/10.1080/19336896.2020.1859439

12. Sun, H. and Marelli, B., Polypeptide templating for designer hierarchical materials, *Nat. Commun*. (2020) **11**, 351. https://doi.org/10.1038/s41467-019-14257-0

13. True, H.L. and Lindquist, S.L., A yeast prion provides a mechanism for genetic variation and phenotypic diversity, *Nature*, 2000, **407**, 477-483. doi: 10.1038/35035005

14. Sievers, S.A., Karanicolas, J., Chang, H.W., Zhao, A., Jiang1, L., Zirafi, O., Stevens, J.T., Münch, J., Baker, D., and Eisenberg, D., Structure-Based Design of Non-Natural Amino Acid Inhibitors of Amyloid Fibrillation, *Nature*. 2014, 475(7354), 96–100. doi:10.1038/nature10154.

379 15. Kumar, V.A., Wang, B.K., and Kanahara, S.M., Rational design of fiber forming
380 supramolecular structures, *Experiment. Biol. Med*. 2016, **241**, 899–908. DOI:
381 10.1177/1535370216640941
382 16. Haspel, N., Zheng, J., Aleman, C., Zanuy, D., Nussinov, R., A Protocol for the Design of
383 Protein and Peptide Nanostructure Self-Assemblies Exploiting Synthetic Amino Acids, *Methods*
384 *Mol Biol*. 2017, **1529**, 323–352. doi:10.1007/978-1-4939-6637-0_17.
385 17. Das, S., Jacob, R.S., Patel, K., Singh, N., and Maji, S.K., Amyloid Fibrils: Versatile
386 Biomaterials for Cell Adhesion and Tissue Engineering Applications, *Biomacromolecules* 2018,
387 **19**, 1826−1839. DOI: 10.1021/acs.biomac.8b00279
388 18. Hilderbrand, A.M., Ford, E.N., Guo, C., Sloppy, J.D., and Kloxin, A.M., Hierarchically
389 structured hydrogels utilizing multifunctional assembling peptides for 3D cell culture, *Biomater.*
390 *Sci*., 2020, **8**, 1256-1269. DOI: 10.1039/c9bm01894h
391 19. Kokotidou C, Jonnalagadda, S.V.R., Orr, A.A., Vrentzos, G., Kretsovali, A., Tamamis, P., and
392 Mitraki, A., Designer Amyloid Cell-Penetrating Peptides for Potential Use as Gene Transfer
393 Vehicles, *Biomolecules* 2020, **10**, 7; doi:10.3390/biom10010007
394 20. Barros, S.M., Whitaker, S.K., Sukthankar, P., Avila, L.A., Gudlur, S., Warner, M., Beltrão,
395 E.I.C., and Tomich, J.M., A Review of Solute Encapsulating Nanoparticles used as Delivery
396 Systems with Emphasis on Branched Amphipathic Peptide Capsules, *Arch Biochem Biophys*.

2016, **596**, 22–42. doi:10.1016/j.abb.2016.02.027.

21. Liu, R., Zhao, J., Han, Q., Hu, X., Wang, D., Zhang, X., and Yang, P., One-Step Assembly of a Biomimetic Biopolymer Coating for Particle Surface Engineering, *Adv. Mater*. 2018, **30**, 1802851. DOI: 10.1002/adma.201802851

22. Li, C., Qin, R., Liu, R., Miao, S., and Yang, P., Functional amyloid materials at surfaces/interfaces, *Biomater. Sci.*, 2018, **6**, 462. DOI: 10.1039/c7bm01124e

23. Li, L., Darden, T.A., Bartolotti, L., Kominos, D., and Pedersen, L.G., An Atomic Model for the Pleated β-Sheet Structure of Aβ Amyloid Protofilaments, *Biophys. J.*, 1999, **76**, 2871–2878. doi: 10.1016/S0006-3495(99)77442-4

24. Do, T.D., LaPointe, N.E., Sangwan, S., Teplow, D.B., Feinstein, S.C., Sawaya, M.R., Eisenberg, D.S., and Bowers, M.T., Factors That Drive Peptide Assembly from Native to Amyloid Structures: Experimental and Theoretical Analysis of [Leu-5]-Enkephalin Mutants, *J. Phys. Chem. B*, 2014, **118**, 7247−7256. dx.doi.org/10.1021/jp502473s

25. Deckert-Gaudig, T. and Deckert, V., High resolution spectroscopy reveals fibrillation inhibition pathways of insulin, *Sci. Rep*. 2016, **6**, 39622. doi: 10.1038/srep39622.

26. Ramshini, H. Tayebee, R., Bigi, A., Bemporad, F., Cecchi, C., and Chiti, F., Identification of Novel 1,3,5-Triphenylbenzene Derivative Compounds as Inhibitors of Hen Lysozyme Amyloid Fibril Formation, *Int. J. Mol. Sci.* 2019, **20**, 5558. doi:10.3390/ijms20225558

415 27. Lee, B.Y., Attwood, S.J., Turnbull, S., and Leonenko, Z., Effect of Varying Concentrations of
416 Docosahexaenoic Acid on Amyloid Beta (1–42) Aggregation: An Atomic Force Microscopy
417 Study, *Molecules*, 2018, **23**, 3089. doi:10.3390/molecules23123089
418 28. Pandey, G., Saikia, J., Sasidharan, S., Joshi, D.C., Thota, S., Nemade, H.B., Chaudhary, N.,
419 and Ramakrishnan, V., Modulation of Peptide Based Nano-Assemblies with Electric and
420 Magnetic Fields, *Sci. Rep*., 2017, **7**, 2726. DOI:10.1038/s41598-017-02609-z
421 29. Lee, G., Lee, W., Lee, H., Lee, C.Y., Eom, K., and Kwon, T., Self-assembled amyloid fibrils
422 with controllable conformational heterogeneity, *Sci. Rep*., 2015, **5**, 16220. DOI:
423 10.1038/srep16220
424 30. Hettiarachchi, C.A., Melton, L.D., Gerrard, J.A., and Loveday, S.M., Formation of
425 β-Lactoglobulin Nanofibrils by Microwave Heating Gives a Peptide Composition Different from
426 Conventional Heating, *Biomacromolecules*, 2012, **13**, 2868−2880. doi.org/10.1021/bm300896r
427 31. Yamaguchi, K., Matsumoto, T., and Kuwata, K., Proper calibration of ultrasonic power
428 enabled the quantitative analysis of the ultrasonication-induced amyloid formation process,
429 *Protein Sci*., 2012, **21**, 38-49. doi: 10.1002/pro.755
430 32. Tang, SQ., Du, QH., Fu, Z., Ultrasonic treatment on physicochemical properties of water-
431 soluble protein from Moringa oleifera seed, *Ultrason. Sonochem*. 2021, **71**, 105357.
432 https://doi.org/10.1016/j.ultsonch.2020.105357

433 33. Nibali, V.C., and Havenith, M., New Insights into the Role of Water in Biological Function:
434 Studying Solvated Biomolecules Using Terahertz Absorption Spectroscopy in Conjunction with
435 Molecular Dynamics Simulations, *J. Am. Chem. Soc*., 2014, **136**, 12800−12807.
436 dx.doi.org/10.1021/ja504441h
437 34. Wilmink, G.J., and Grundt, J.E., Invited Review Article: Current State of Research on
438 Biological Effects of Terahertz Radiation, *J. Infrared Milli. Terahz. Waves*, 2011, **32**, 1074–1122.
439 DOI 10.1007/s10762-011-9794-5
440 35. Irizawa, A, Fujimoto, M. Kawase, K., Kato, R., Fujiwara, H., Higashiya, A., Macis, S.,
441 Tomarchio, L., Lupi, S., Marcelli, A., and Suga, S., Spatially Resolved Spectral Imaging by A
442 THz-FEL, *Condens. Matter*, 2020, **5**, 38. doi:10.3390/condmat5020038
443 36. Isoyama, G., Development of a Free-Electron Laser in the Terahertz Region, *JAS4QoL*, 2020,
444 **6**(1), 2:1-10. http://as4qol.org/?p=2894
445 37. Idehara, T., Sabchevski, S.P., Glyavin, M., and Mitsudo, S., The Gyrotrons as Promising
446 Radiation Sources for THz Sensing and Imaging, *Appl. Sci*., 2020, **10**, 980.
447 doi:10.3390/app10030980
448 38. Ryan, H., Bentum, J., and Maly, T., A Ferromagnetic Shim Insert for NMR Magnets – Towards
449 an Integrated Gyrotron for DNP-NMR Spectroscopy, *J. Magn. Reson*., 2017, **277**, 1–7.
450 doi:10.1016/j.jmr.2017.01.021.

39. Nanni, E.A., Barnes, A.B., Griffin, R.G., and Temkin, R.J., THz Dynamic Nuclear Polarization NMR, *IEEE Trans Terahertz Sci. Technol*., 2011, **1**(1), 145–163. doi: 10.1109/TTHZ.2011.2159546

40. Maly, T., Debelouchina, G.T., Bajaj, V.S., Hu, K-N., Joo, C-G., Mak–Jurkauskas, M.L., Sirigiri, J.R., van der Wel, P.C.A., Herzfeld, J., Temkin, R.J., and Griffin, R.G., Dynamic nuclear polarization at high magnetic fields, *J. Chem. Phys*., 2008, **128**(5), 052211. doi:10.1063/1.2833582.

41. Mattsson, M-O., Simkó, M., Emerging medical applications based on non-ionizing electromagnetic fields from 0 Hz to 10 THz, *Medical Devices: Evidence and Research*, 2019, **12**, 347–368. https://doi.org/10.2147/MDER.S214152

42. Kok, H.P., Cressman, E.N.K., Ceelen, W., Brace, C.L., Ivkov, R., Grüll, H., ter Haar, G., Wust, P., and Crezee, J., Heating technology for malignant tumors: a review, *Int. J. Hyperthermia*., 2020, **37**(1), 711–741. doi:10.1080/02656736.2020.1779357

43. Usoltsev, D., Sitnikova, V., Kajava, A., and Uspenskaya, M., Systematic FTIR Spectroscopy Study of the Secondary Structure Changes in Human Serum Albumin under Various Denaturation Conditions, *Biomolecules*, 2019, 9, 359. doi:10.3390/biom9080359

44. Sarver, R. W. Jr. and Krueger, W. C., Protein secondary structure from Fourier transform infrared spectroscopy: a data base analysis. *Anal. Biochem*., 1991, **194**, 89–100.

https://doi.org/10.1016/0003-2697(91)90155-M

45. Narayanan, T. and Konovalov, O., Synchrotron Scattering Methods for Nanomaterials and Soft Matter Research, *Materials*, 2020, **13**, 752. doi:10.3390/ma13030752

46. Iwata, K., Fujiwara, T., Matsuki, Y., Akutsu, H., Takahashi, S., Naiki, H., and Goto, Y., 3D structure of amyloid protofilaments of β2-microglobulin fragment probed by solid-state NMR, *Proc. Nat. Aca. Sci*., 2006, **103**(48), 18119–18124. Doi/10.1073/pnas.0607180103

47. Kawasaki, T., Yamaguchi, Y., Ueda, T., Ishikawa, Y., Yaji, T., Ohta, T., Tsukiyama, K., Idehara, T., Saiki, M., and Tani, M., Irradiation effect of a submillimeter wave from 420 GHz gyrotron on amyloid peptides in vitro, *Biomed. Opt. Express*, 2020, **11**(9), 5341-5351. doi.org/10.1364/BOE.395218

48. Kawasaki, T., Tsukiyama, K., and Irizawa, A., Dissolution of a fibrous peptide by terahertz free electron laser, *Sci. Rep*., 2019, **9**, 10636. https://doi.org/10.1038/s41598-019-47011-z

49. Lee, B.Y., Attwood, S.J., Turnbull, S. and Leonenko, Z., Effect of Varying Concentrations of Docosahexaenoic Acid on Amyloid Beta (1–42) Aggregation: An Atomic Force Microscopy Study, Molecules 2018, 23, 3089; doi:10.3390/molecules23123089.

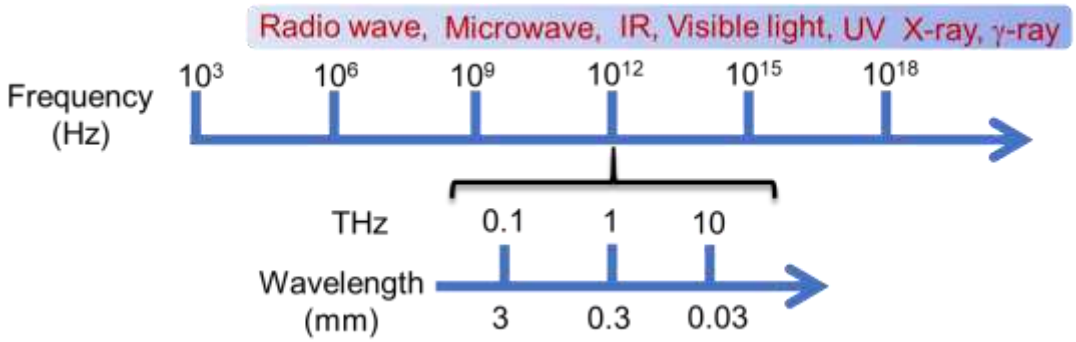

Oscillation system	Wavelength	Irradiation Power	Pulse duration
THz-FEL	30 – 300 μm	avg. 5 mJ /macro-pulse	4 μs (macro-pulse) 20 ps (micro-pulse)
Gyrotron	0.3 – 3 mm	10 W	1-2 ms

Fig. 1a

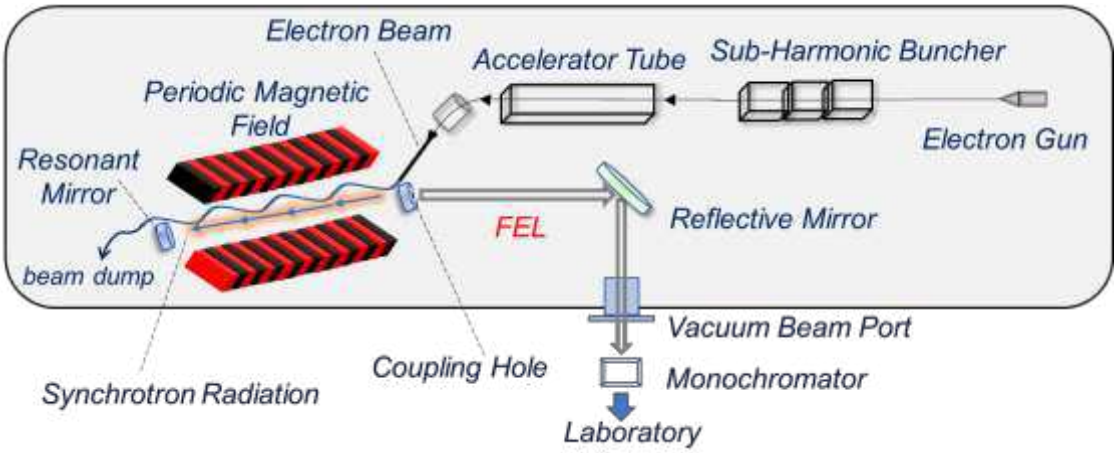
Electron Beam
Accelerator Tube
Sub-Harmonic Buncher
Periodic Magnetic Field
Electron Gun
Resonant Mirror
FEL
Reflective Mirror
beam dump
Vacuum Beam Port
Coupling Hole
Monochromator
Synchrotron Radiation
Laboratory

Fig. 1b

513

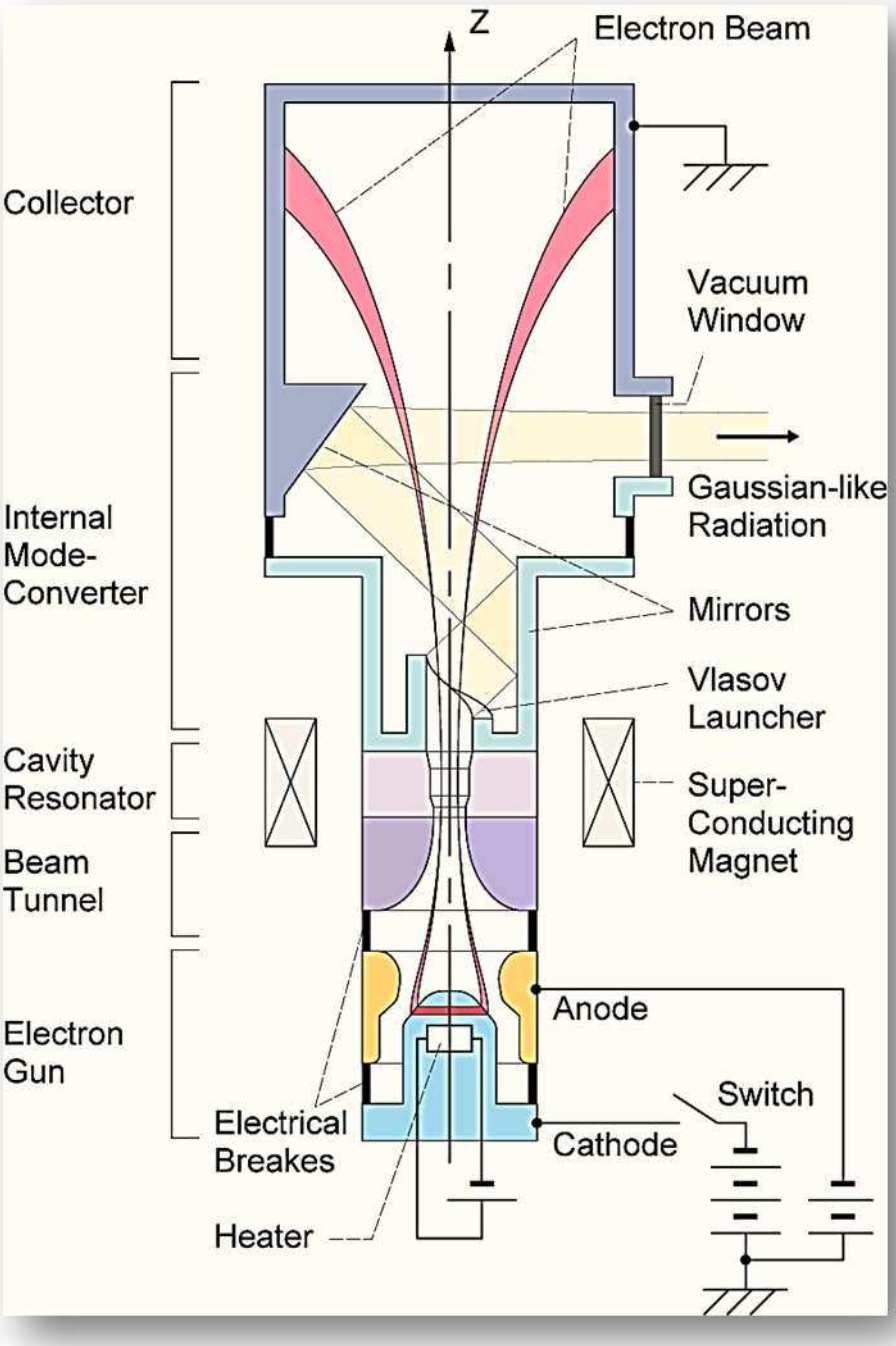

514

515

516 **Fig. 1c**

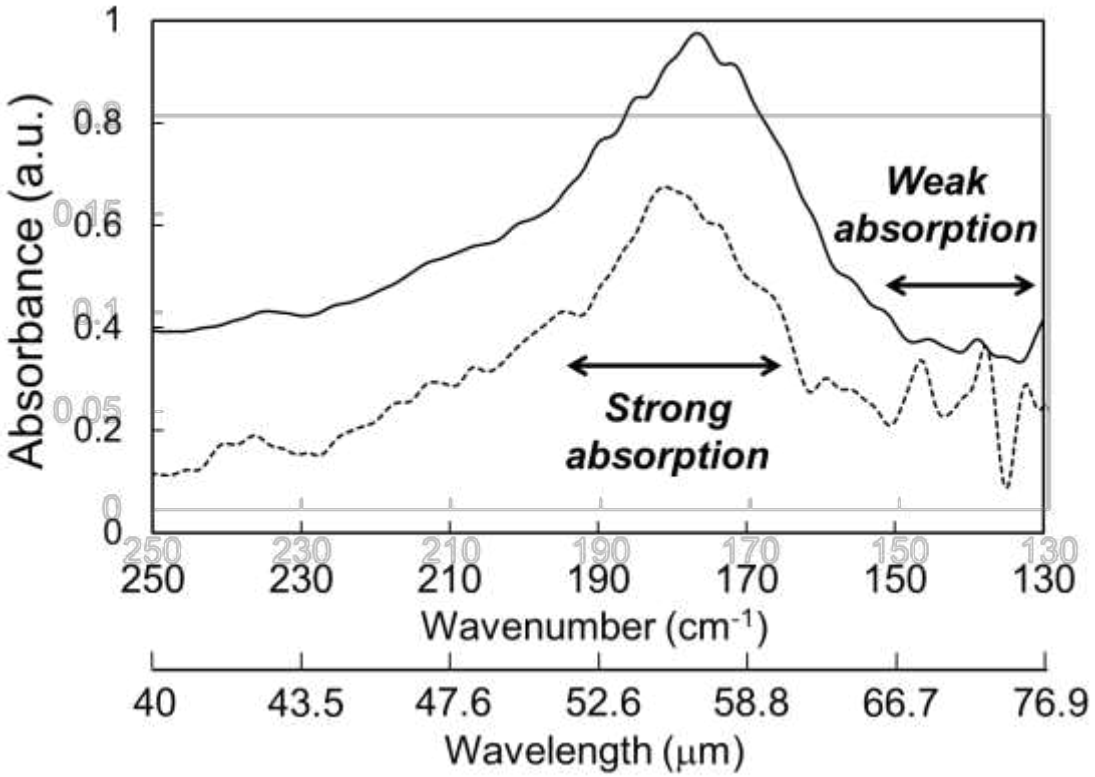
Absorbance (a.u.)
1
0.8
0.6
0.4
0.2
0
Weak
absorption
Strong
absorption
250
230
210
190
170
150
130
Wavenumber (cm-1)
40
43.5
47.6
52.6
58.8
66.7
76.9
Wavelength (μm)

Fig. 2a

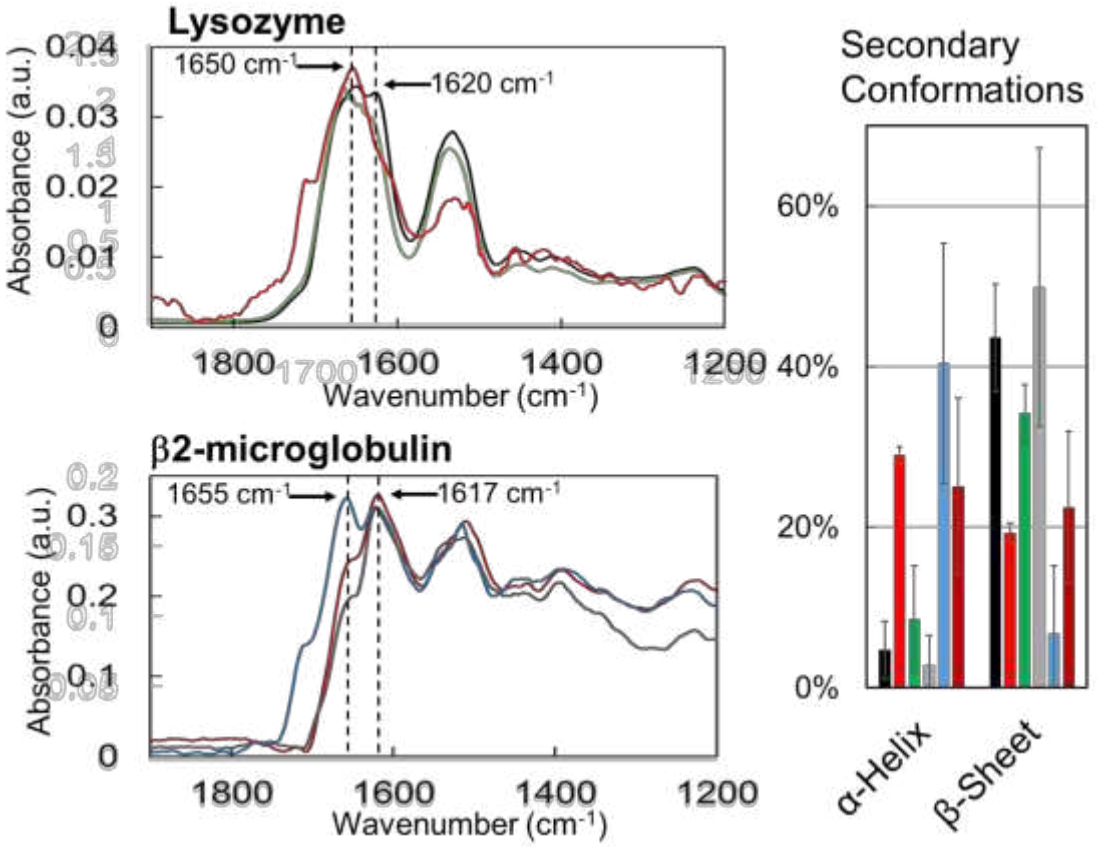
Lysozyme
1650 cm-1
1620 cm-1
Absorbance (a.u.)
0.04
0.03
0.02
0.01
0
1800
1600
1400
1200
Wavenumber (cm-1)
β2-microglobulin
1655 cm-1
1617 cm-1
Absorbance (a.u.)
0.3
0.2
0.1
0
1800
1600
1400
1200
Wavenumber (cm-1)
Secondary Conformations
60%
40%
20%
0%
α-Helix
β-Sheet

Fig. 2b

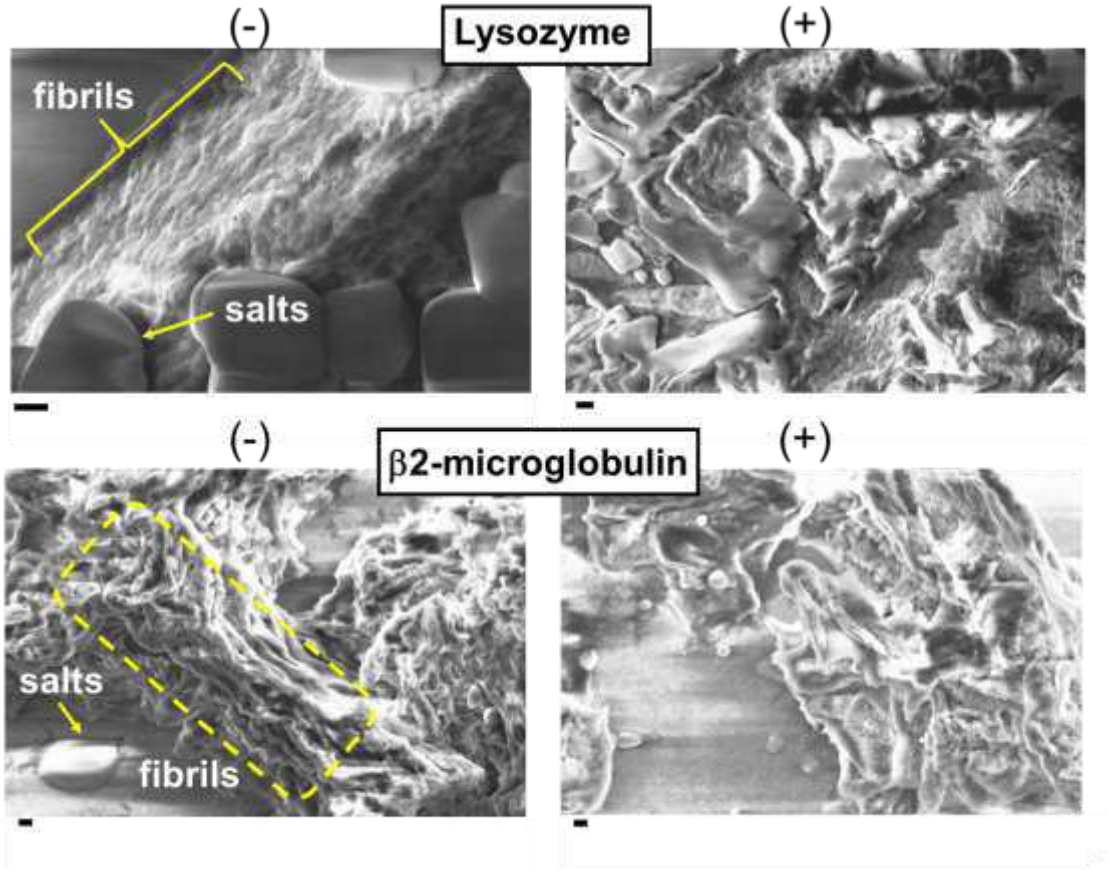

Fig. 2c

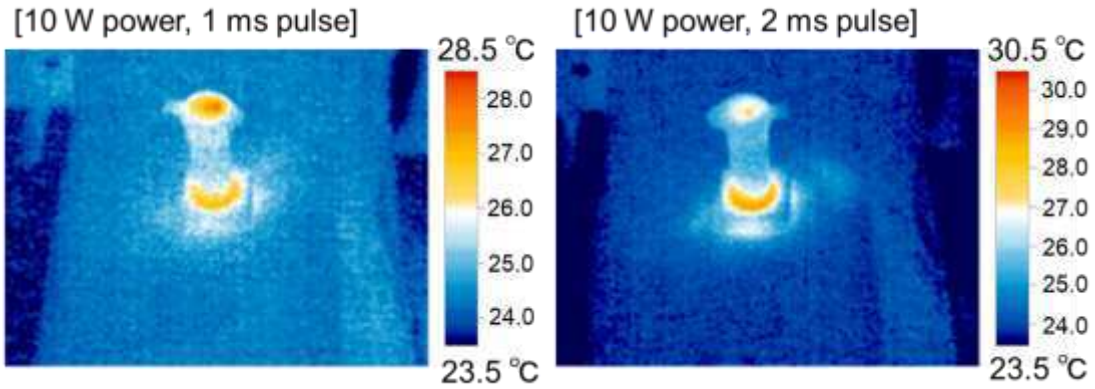
[10 W power, 1 ms pulse]
28.5 °C
28.0
27.0
26.0
25.0
24.0
23.5 °C
[10 W power, 2 ms pulse]
30.5 °C
30.0
29.0
28.0
27.0
26.0
25.0
24.0
23.5 °C

Fig. 3a

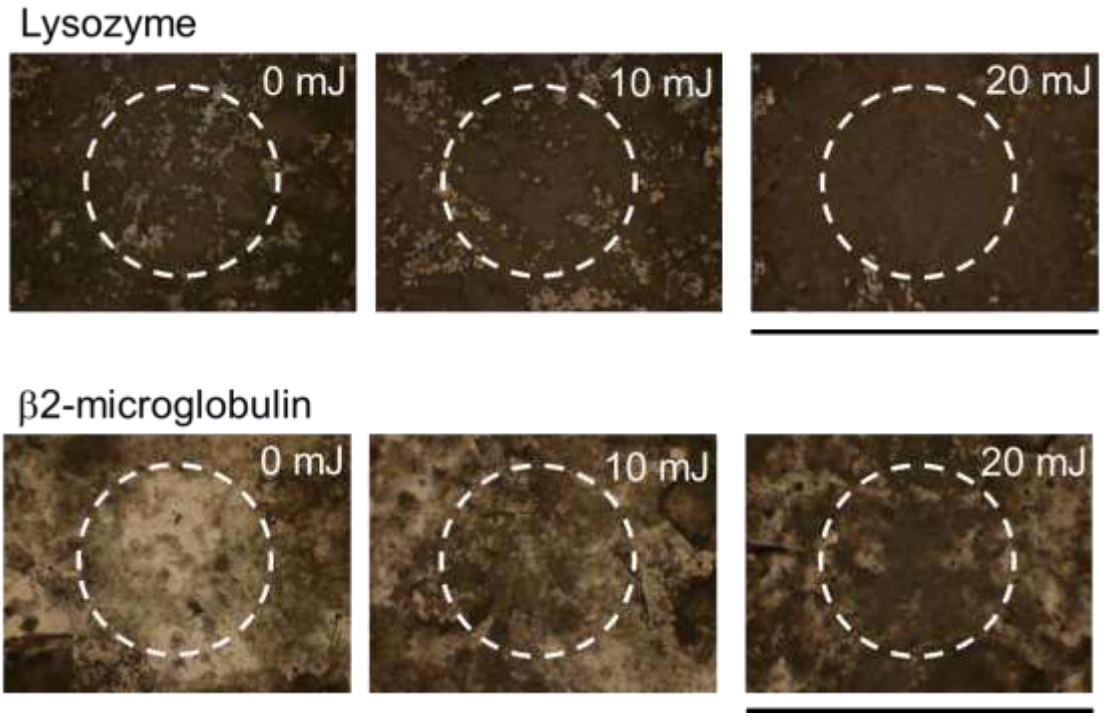

Fig. 3b

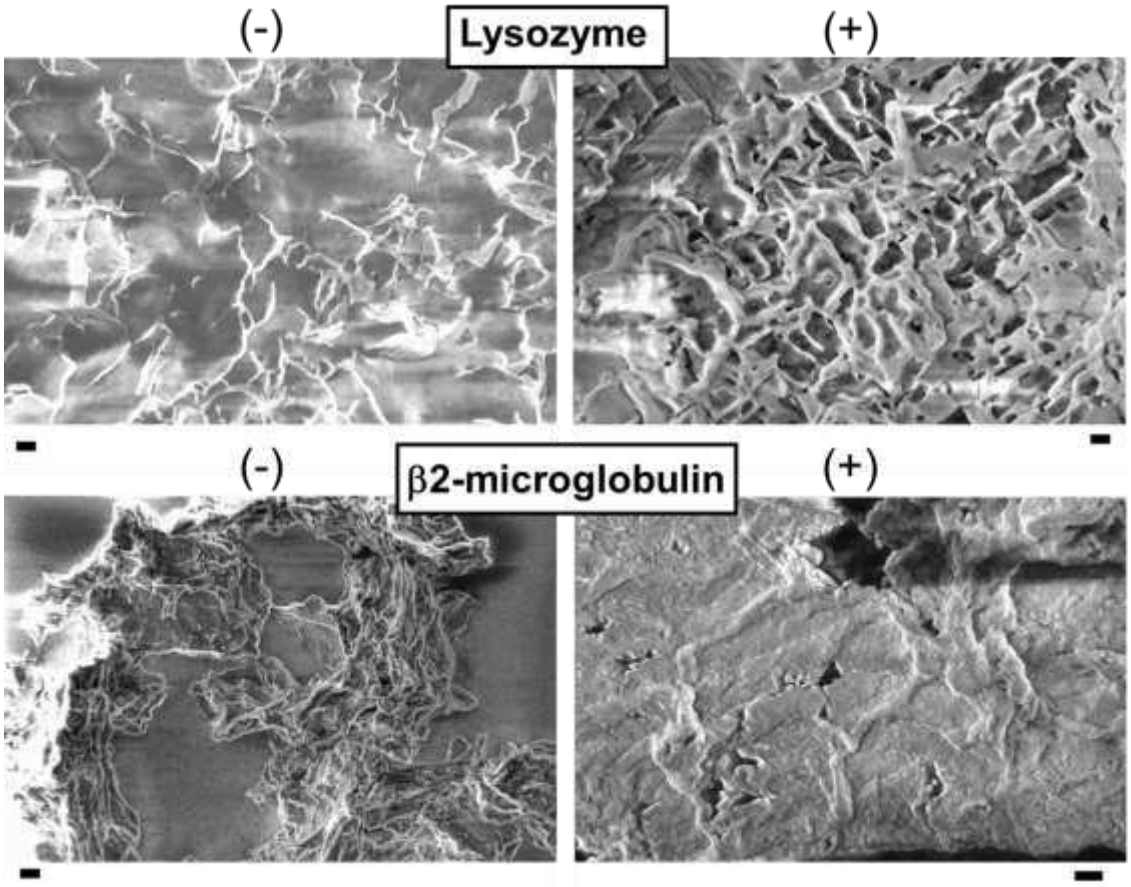

Fig. 3c

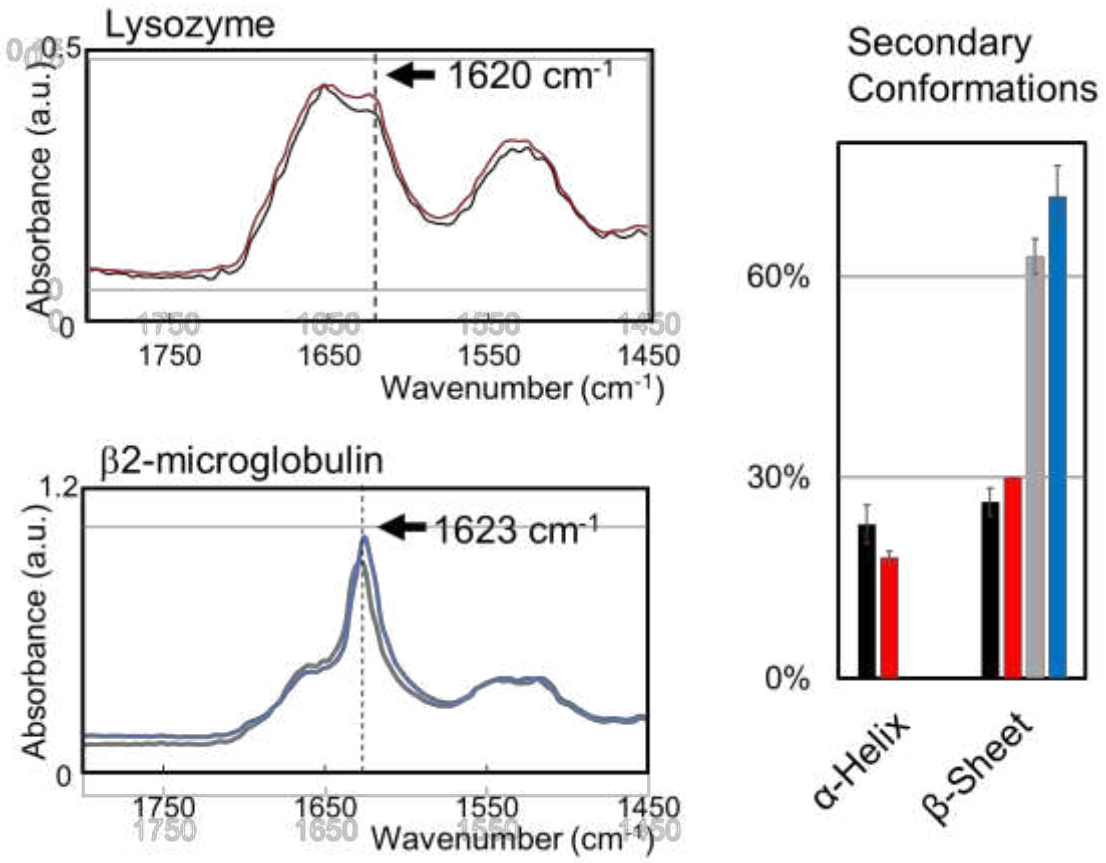
Lysozyme
0.5
0
Absorbance (a.u.)
1620 cm-1
1750
1650
1550
1450
Wavenumber (cm-1)
β2-microglobulin
1.2
0
Absorbance (a.u.)
1623 cm-1
1750
1650
1550
1450
Wavenumber (cm-1)
Secondary Conformations
60%
30%
0%
α-Helix
β-Sheet

Fig. 3d

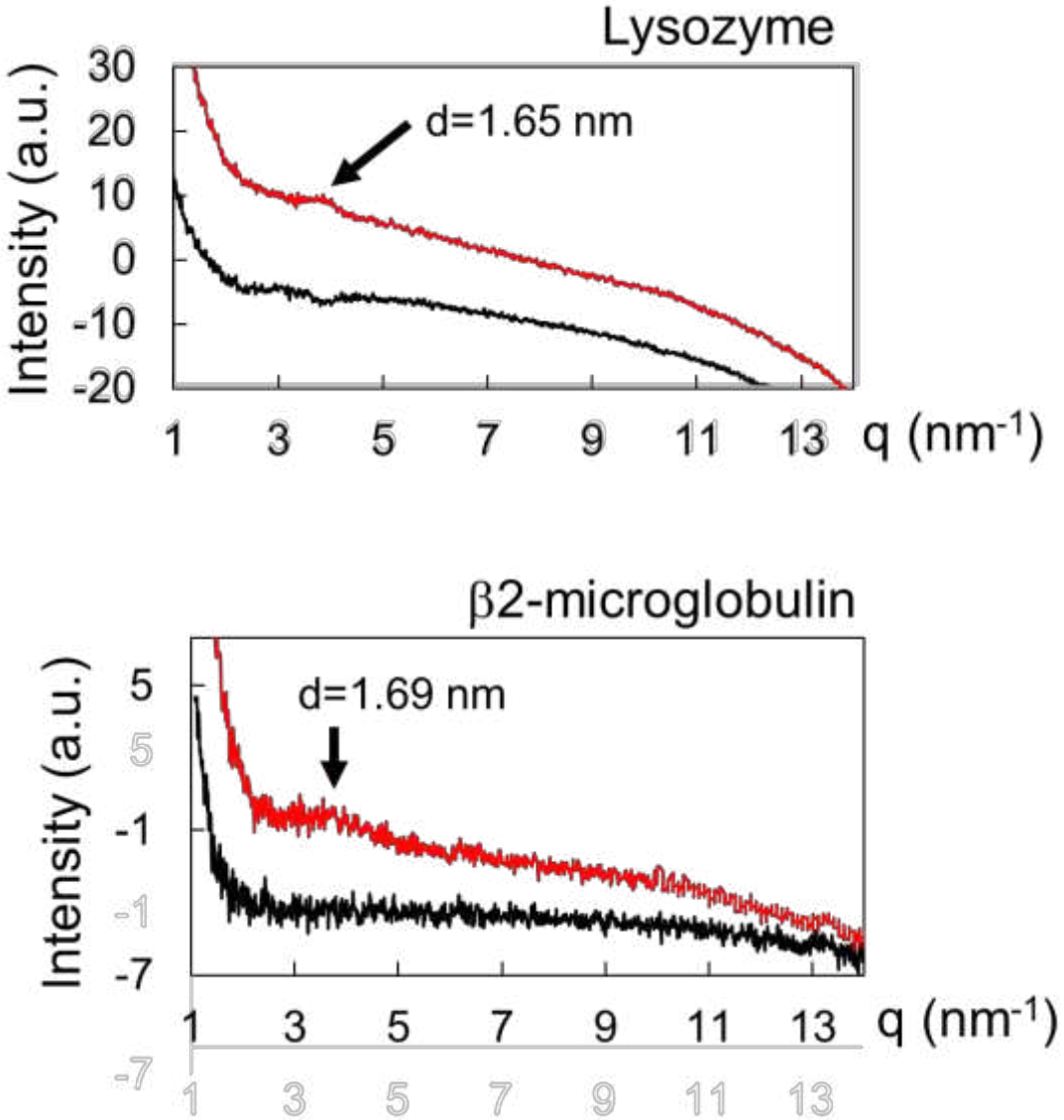
Lysozyme
Intensity (a.u.)
30
20
10
0
-10
-20
d=1.65 nm
1
3
5
7
9
11
13
q (nm-1)
β2-microglobulin
Intensity (a.u.)
5
-1
-7
d=1.69 nm
1
3
5
7
9
11
13
q (nm-1)

Fig. 3e

600

601

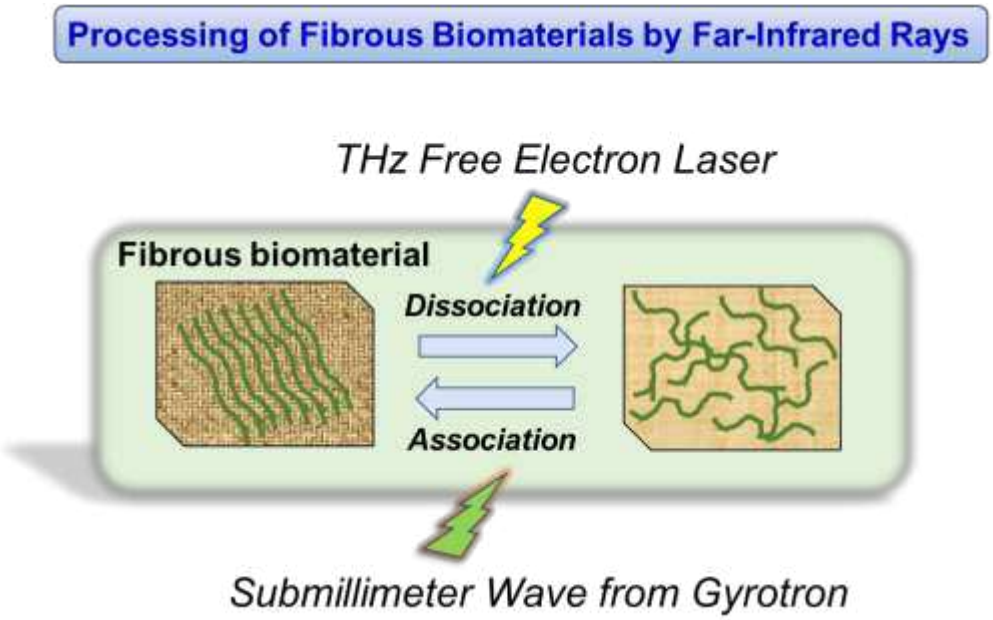

602

603

604 **Fig. 4**

Supplementary Files

This is a list of supplementary files associated with this preprint. Click to download.

- SupportingInformation0730Kawasaki.pdf